

Recrystallization and grain growth activation energies in a hybrid magnesium material fabricated by high-pressure torsion

Hiba Azzeddine^{1,*}, Marie-Noëlle Avettand-Fènoël², Piotr Bazarnik³, Thierry Baudin⁴,
Yi Huang^{5,6}, Terence G. Langdon⁵

¹ Laboratory of Materials and Renewable Energy, Faculty of Sciences, Mohamed Boudiaf University, 28000 M'sila, Algeria

² Univ. Lille, CNRS, INRAE, Centrale Lille, UMR 8207, UMET - Unité Matériaux Et Transformations, F-59000 Lille, France

³ Warsaw University of Technology, Faculty of Materials Science and Engineering, Woloska 141, 02-507, Poland

⁴ Université Paris-Saclay, CNRS, Institut de chimie moléculaire et des matériaux d'Orsay, 91405 Orsay, France

⁵ Materials Research Group, Department of Mechanical Engineering, University of Southampton, Southampton SO17 1BJ, UK

⁶ Department of Design and Engineering, Faculty of Science and Technology, Bournemouth University, Poole, Dorset BH12 5BB, UK

* Corresponding author: Prof. Hiba Azzeddine, hiba.azzeddine@univ-msila.dz

Abstract

The recrystallization and grain growth activation energies of the hybrid AZ31/Mg-0.6Gd (wt.%) alloy were calculated using differential scanning calorimetry analyses and scanning electron microscopy, respectively, after fabricating by high-pressure torsion up to 20 turns and then subjecting to an isochronal annealing treatment from 423 to 723 K for 1 h. The DSC results show one exothermic peak belonging to the static recrystallization of the AZ31 region with an activation energy of 112 ± 10 kJ/mol. The grain growth kinetics for the AZ31 and Mg-0.6Gd regions were described by the Arrhenius equation. The calculation with a grain growth exponent equal to 4 gave values for the activation energies in both the AZ31 (146.2 ± 8.4 kJ/mol) and Mg-0.6Gd (90.9 ± 13.5 kJ/mol) regions. The present results reveal the heterogeneity of the thermal stability of the AZ31/Mg-0.6Gd hybrid material.

Keywords: Activation energy; Grain growth; High-pressure torsion; Magnesium; Recrystallization.

1. Introduction

At the present time the use of metal-matrix composites is gradually increasing in various industries such as transportation and construction owing to their superior properties compared to the use of single materials [1]. From an economic and environmental point of view, magnesium (Mg) based composites attract much attention from both the academic and industrial communities due to their combination of high strength and lightweight structure [2]. Moreover, the biocompatibility and biodegradable characteristics of Mg-based alloys make them excellent potential candidate materials for use in biological applications such as temporary implants [3-5].

Severe plastic deformation (SPD) techniques, particularly processing by high-pressure torsion (HPT), is now considered one of the most effective production routes for fabricating metal-matrix composites at room temperature (RT) [6]. In the production of bulk ultrafine-grained materials, the high hydrostatic compressive stress combined with high shear deformation under HPT processing permit the successful bonding of particles through a solid state reaction without any sample cracking. For example, dense bulk Mg-Al₂O₃ and Mg-hydroxyapatite composites were produced with better mechanical properties and corrosion resistance than pure Mg by applying HPT processing through 5 turns at a pressure of 6 GPa [7-9] and the production of dense AZ91-Al₂O₃ composite bulk discs needed 20 turns of HPT processing at the same pressure of 6 GPa [10]. By contrast, HPT processing through 50 turns failed to consolidate an AZ91-bioactive glass composite due to sliding between the particles and strain localization [8].

Processing by HPT is important also for producing Mg hybrid materials by stacking different discs together including Al/Mg [11-14], Zn/Mg [15-18] and the AZ31(Mg-3Al-1Zn, wt.)/Mg-0.6Gd (wt.%) [19-21] systems. Diffusion bonding induced by HPT processing is capable of improving the mechanical properties of the hybrid systems by a combination of grain refinement and the creation of microstructural heterogeneities such as a segregation of alloying elements at defects, precipitation and the formation of unexpected intermetallic phases at RT [15, 16, 20].

Despite the numerous reports describing the fabrication of new generations of Mg-based composites [7-21], neither the deformation and the thermal stability behaviour nor the corresponding mechanisms controlling the microstructural evolution and mechanical properties of these composites are fully understood. This is a significant limitation since the recrystallization and grain growth kinetics of composite materials is a key factor for controlling

their mechanical properties in order to meet the requirements for industrial applications. Accordingly, the present research was initiated to contribute towards this understanding by determining the activation energies for recrystallization and grain growth in a hybrid AZ31-Mg-0.6Gd (wt.%) material by fabricating using HPT processing for 20 turns under a pressure of 6.0 GPa.

2. Experimental material and procedures

AZ31 and Mg-0.6Gd discs of 10 mm diameter and 0.85 mm thickness were processed together by HPT at RT for a total of 20 turns under an applied pressure of 6.0 GPa using a rotational speed of 1 rpm and quasi-constrained conditions [22]. The HPT-processed discs were then exposed to isochronal annealing for 1 h at 423, 523, 623 and 723 K in a radiation furnace. More details on the AZ31 and Mg-0.6Gd alloys, and specifically the microstructural evolution and mechanical properties of the hybrid material under HPT processing and annealing conditions, were given in earlier reports [19-21].

Microstructural observations near the AZ31 and Mg-0.6Gd interface of the annealed samples were performed using a scanning electron microscope (SEM) Hitachi Su8000, Hitachi High-Tech corporation, Tokyo, Japan, operating in back-scattered electron (BSE) mode. Complementary microstructural observations on the AZ31 and Mg-0.6Gd regions of the annealed samples at 523 and 623 K were performed in bright-field (BF) and high-angle annular dark field (HAADF) modes using a scanning transmission electron microscope (STEM) Spectra 200, Thermo Fisher Scientific, Massachusetts, U.S., operating at an accelerating voltage of 200 kV. Structural investigations were combined with advanced energy dispersive X-Ray (EDX) point and mapping analyses. More details on the sample preparations for SEM and STEM characterization are given elsewhere [20].

The DSC analyses were performed using alumina crucibles in a DSC 404 calorimeter Netzsch GmbH, Dardilly, France, under an Argon atmosphere and over a temperature range between 298 and 623 K. The DSC analyses of the processed hybrid material with a mass of 15.5 mg were conducted with constant heating rates of 5, 10 and 15 K/min. For comparison, DSC scans under a heating rate of 10 K/min were performed for the AZ31 (18.6 mg) and Mg-0.6Gd (12.6 mg) alloys processed by HPT separately for 20 turns.

3. Experimental results and discussion

3.1. Recrystallization activation energy

Figure 1a shows the DSC curves of the hybrid material at heating rates of 5, 10 and 15 K/min. All curves display one exothermic (heat-releasing) peak (named 1) corresponding to the recrystallization process and one endothermic (heat-absorbing) peak (named 2) indicating the dissolution of precipitates. Figure 1b shows the DSC curves at a heating rate of 10 K/min for the AZ31 and Mg-0.6Gd alloys after HPT processing separately. As can be seen, the DSC curve of the HPT-processed AZ31 alloy shows the presence of one exothermic peak and a small endothermic peak is evident in the enlarged curve between 593 and 423 K shown in Figure 1b. In this case, the exothermic peak is attributed to a static recrystallization process and the endothermic peak corresponds to the dissolution of the $Mg_{17}Al_{12}$ phase. The peak temperature for the dissolution of this phase is around 639 K which is lower than the usual report of 684 K for the AZ31 alloy [23]. This reduction in the dissolution temperature is mainly attributed to the effect of the severe plastic deformation. Indeed, the large numbers of grain boundaries resulting from the grain refinement and the high density of dislocations and vacancies induced by the SPD processing strongly disturbs the mobility of the solute atoms and therefore affects the sequence and precipitation kinetics [24-26]. By contrast, the DSC curve of the HPT-processed Mg-0.6Gd alloy in Figure 1b indicates the presence of only one endothermic peak which is consistent with the dissolution of phases. Based on the equilibrium phase diagram of the Mg-Gd system, these could be the Mg_5Gd and $Mg_{12}Gd$ phases [27]. The absence of an exothermic peak for the Mg-0.6Gd alloy, even if the alloy undergoes HPT processing, is explained since the grains were already recrystallized during deformation due to the occurrence of extensive dynamic recrystallization (DRX). Indeed, it was reported earlier that DRX was enhanced in the Mg-0.6Gd alloy (80%) by comparison with the AZ31 alloy (58%) under HPT processing [19, 28]. It must be mentioned that, unlike the traditional AZ31 alloy, the DRX process is usually retarded in RE-containing Mg alloys during thermomechanical processing such as extrusion [29], hot-rolling [30, 31] and plane strain compression [32-34]. It is believed that the RE elements play a key role by pinning the grain boundary mobility and reducing the stacking fault energy of the alloy which changes significantly the recovery process [30, 35]. However, the reversal deformation behavior between AZ31 and Mg-0.6Gd alloys during HPT processing was related to the manner in which the alloys stored the energy induced by the high strain, the amount and the distribution of second phases (stable nano-sized $Mg_{17}Al_{12}$ and Al_8Mn_5 phases vs. the fragmentation of Mg_5Gd phase) and the concentration of alloying elements (3% Al and 1% Zn vs. 0.6% Gd element) [28].

Thus, it is concluded that the exothermic peak shown in the hybrid material in Figure 1a is essentially due to the recrystallization of the AZ31 region while the endothermic peak is due to a combined precipitate dissolution of the $Mg_{17}Al_{12}$ and $Mg_5Gd/Mg_{12}Gd$ phases in both the AZ31 and Mg-0.6Gd regions, respectively. In the following, therefore, only the recrystallization peak is taken into account and the dissolution of the precipitate phases remains a subject for future investigation.

Figure 1c presents the recrystallization peak after baseline subtraction of the hybrid material at heating rates of 5, 10 and 15 K/min. The corresponding values of the maximum temperature of the recrystallization peak, T_p , increases with increasing heating rate in the sequence of 150, 433 and 440 K at 5, 10 and 15 K/min, respectively. The shifting of the recrystallization peak towards higher temperatures with increasing heating rate means that the recrystallization phenomenon is a thermally-activated process. It is important to note that comparable findings were also reported for deformed Mg-based alloys such as the hot-rolled Mg-1.3La (wt.%) [31], HPT-processed Mg-1.4Nd (wt.%) [36] and Mg-0.4Dy (wt.%) [37] alloys.

The Boswell-Kissinger method was used to evaluate the activation energy for recrystallization according to the following equation [38]:

$$\ln\left(\frac{V}{T_p}\right) = C - \frac{E_a}{RT_p} \quad (1)$$

where V is the heating rate, C is a constant, R is the universal gas constant and E_a is the activation energy for recrystallization. It follows that the value of E_a corresponds to the slope of $\ln(V/T_p)$ plotted as a function of $1000/RT_p$ of the recrystallization peak of the hybrid material, as shown in Figure 1d.

The activation energy for recrystallization of the hybrid material was estimated as 112 ± 10 kJ/mol which falls between the activation energy for boundary self-diffusion in Mg (~ 92 kJ/mol) [39] and the activation energy for lattice self-diffusion in Mg (~ 135 kJ/mol) [39]. Based on the reported results, the activation energy for recrystallization in the AZ31 alloy under conventional deformation such as hot-rolling and cold-drawing is in the range of 69-88 kJ/mol [40-42]. It is interesting to note the activation energies for recrystallization in these earlier reports [40-42] were obtained by means of the Johnson-Mehl-Avrami-Kolmogorov model where isothermal annealing treatments were performed. For example, an activation energy of 85.9 kJ/mol was estimated for the cold-drawn AZ31 alloy at annealing temperatures ranging from 483 to 573 K and holding times ranging from 30 min to 8 h [40].

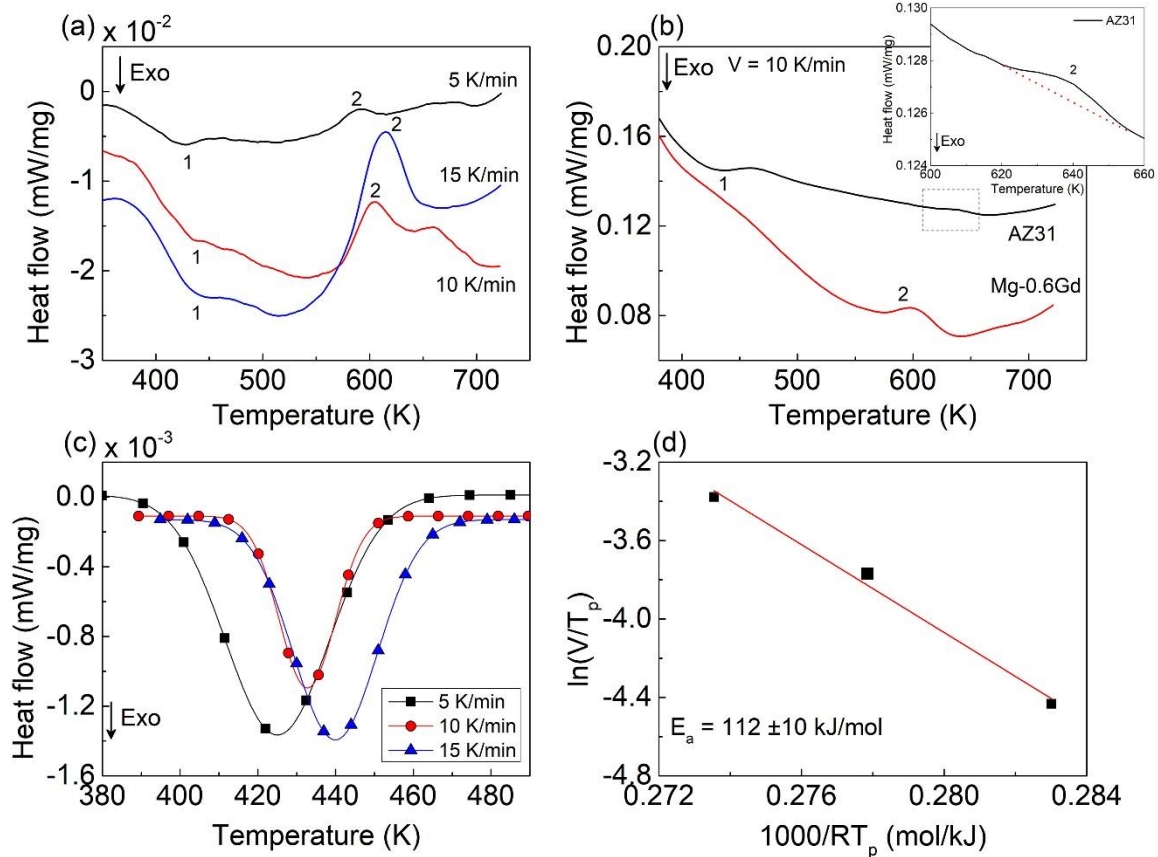


Figure 1: (a) DSC curves of hybrid material measured at heating rates of 5, 10 and 15 K/min, (b) DSC curves measured at a rate of 10 K/min for separate HPT-processed AZ31 and Mg-0.6Gd alloys, (c) recrystallization peak with baseline subtraction of the hybrid material at heating rates of 5, 10 and 15 K/min and (d) determination of the activation energy for recrystallization of the hybrid material.

It was demonstrated earlier that the presence of nano-sized Al_8Mn_5 (~10 nm) and $Mg_{17}Al_{12}$ (~10-40 nm) phases in the microstructure of the HPT-processed AZ31 alloy inhibited the grain boundary motion during the annealing treatments leading to a delay for the static recrystallization process [20]. It is believed that the relative high activation energy obtained for the static recrystallization process is a consequence of the presence of second phases and is indicative of the good thermal stability of the hybrid material.

The activation energy for recrystallization in HPT-processed Mg-1.4Ce (wt.%) alloy calculated by DSC analysis was found to decrease with increasing numbers of HPT turns and the values range from 87.48 to 72.33 kJ/mol for $N = 1/2$ and 10 turns, respectively [43]. The decrease in activation energy was attributed to the increase in stored energy and the number of recrystallization nucleation sites, such as grain boundaries and dislocations, with increasing

numbers of HPT turns [36, 43]. A similar observation was reported for the hot-rolled Mg-1.3La (wt.%) alloy, where the activation energy decreased slightly from 112 to 97 kJ/mol after 20 and 50% of thickness reduction, respectively [31].

3.2. Grain growth activation energy

Figure 2 shows SEM images near the AZ31 and Mg-0.6Gd interfaces of the hybrid material after isochronal annealing for 1 h at 423, 523, 623 and 723 K. The interface between the AZ31 and Mg-0.6Gd regions are identified by dashed yellow lines in each SEM micrograph. The corresponding mean grain size in the annealed AZ31 and Mg-0.6Gd regions is displayed in Figure 2e where the linear intercept method was used to determine these mean grain sizes.

In addition, EDS mapping for Al, Zn and Mn elements of selected areas in the AZ31 region annealed at 523 K (Figure 2b) shows the $Mg_{17}Al_{12}$, Mg_2Zn and Al_8Mn_5 phases and the STEM image in the HAADF mode of the selected area in the Mg-0.6Gd region annealed at 623 K shows $Mg_{12}Gd$ and Mg_5Gd phases (Figure 2c).

The mean grain sizes based on the SEM micrographs of the AZ31 and Mg-0.6Gd regions after HPT processing was reported earlier as 0.30 ± 0.03 and 0.34 ± 0.02 μm , respectively [19]. As can be seen from Figures 2a and 2e, the grain size of the AZ31 region increased after annealing at 423 K to $\sim 1.1 \pm 0.5$ μm and then decreased after annealing at 523 K to $\sim 0.35 \pm 0.6$ μm because of the precipitation of a large $Mg_{17}Al_{12}$ phase (~ 50 -90 nm) and a small (~ 40 nm) phase as evident in the EDS map shown in Figure 2b. As mentioned above, the deformation microstructure of the AZ31 region exhibited already nano-sized Al_8Mn_5 and $Mg_{17}Al_{12}$ particles [19, 28]. In practice, the presence of these nano-sized particles was the main reason for restricting the DRX in the HPT-processed AZ31 alloy [19, 28]. Figure 2c and the results reported previously [20] show that precipitation does not develop in the AZ31 region after annealing at 623 and 723 K and this leads to grain growth.

In the case of the Mg-0.6Gd region, the grain size increased slowly from $\sim 0.41 \pm 0.2$ to $\sim 0.75 \pm 0.2$ μm after annealing at 423 and 523 K, respectively. Subsequently, the microstructure exhibits a notable grain growth at higher temperatures. The mean grain size increases significantly at an annealing temperature of 623 K to $\sim 2.10 \pm 0.7$ μm even with extensive precipitation of the Mg_5Gd and $Mg_{12}Gd$ phases as shown in Figure 2c and the HAADF image within the red frame. Based on the HAADF image, the Mg_5Gd phase is located along the grain boundaries while $Mg_{12}Gd$ particles with an approximately spherical shape and a diameter of ~ 20 nm are distributed within the grains. This precipitation does not restrict the grain boundary

mobility as observed in the AZ31 region which suggests that the Mg_5Gd and $Mg_{12}Gd$ phases probably precipitated after completing the recrystallization and grain growth processes.

Based on the Mg-Gd phase diagram [27], the Mg_5Gd and $Mg_{12}Gd$ phases are not expected to precipitate in an Mg-Gd alloy containing 0.6% of Gd element. Furthermore, the development of the Mg_2Zn phase was never reported in the AZ31 alloy. It was suggested that the combination of the high strain induced by HPT processing and the formation of the interface bonding by solid diffusion is the origin of the unexpected precipitations in both the AZ31 and Mg-0.6Gd regions [20]. Indeed, the fabrication of the hybrid AZ31/Mg-0.6Gd material by HPT processing allows both the AZ31 and Mg-0.6Gd regions to store high energies in the form of high dislocation densities, vacancies or grain boundaries which can promote solute diffusion and provide nucleation sites for precipitate phases. The enhancement of precipitation phenomena by HPT processing is widely reported in Mg-based alloys [18, 44-47].

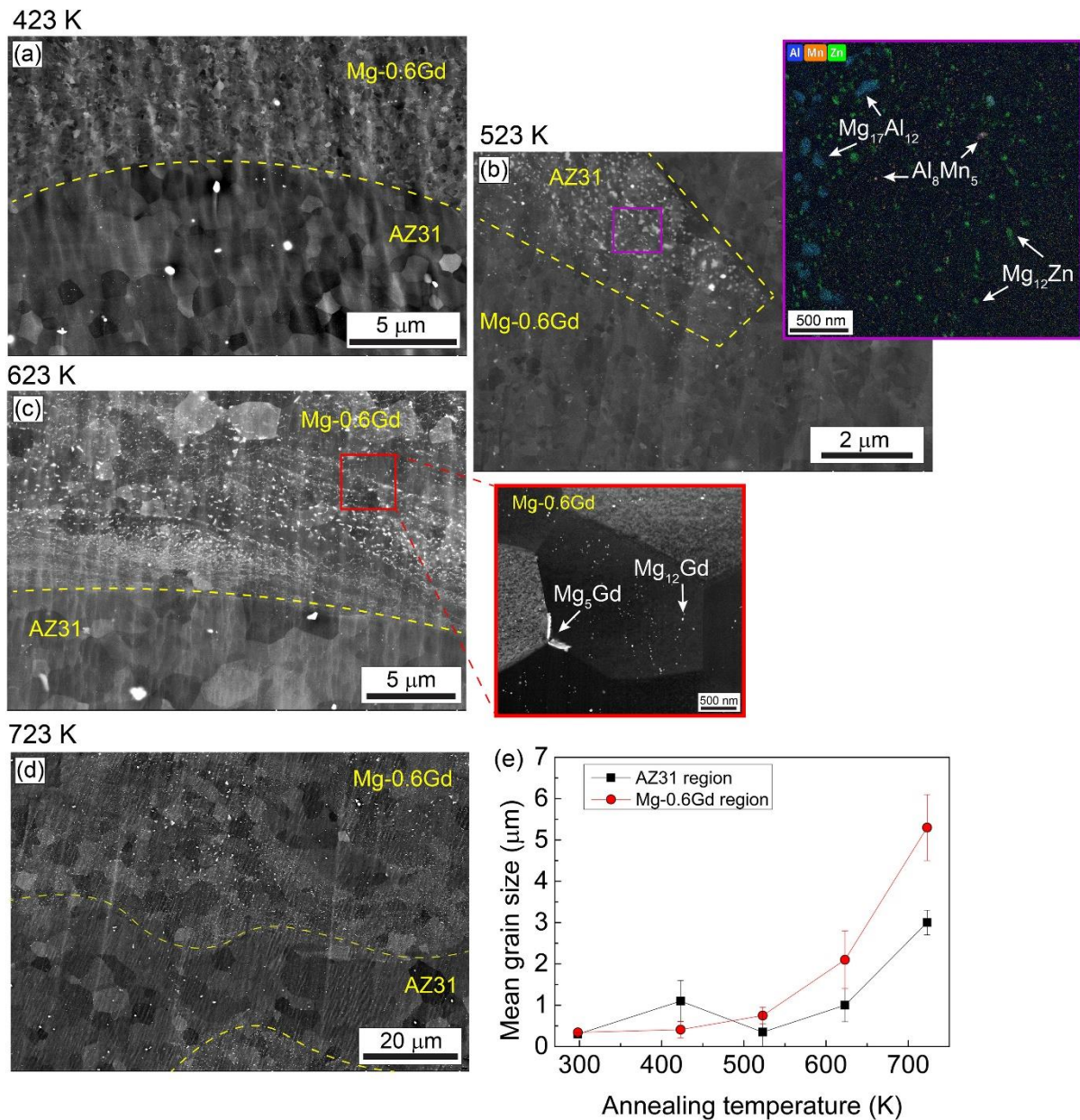


Figure 2: SEM micrographs near the AZ31/Mg-0.6Gd interfaces after annealing for 1 h at (a) 423, (b) 523, (c) 623, and (d) 723 K, (e) evolution of the mean grain size of the AZ31 and Mg-0.6Gd regions as a function of annealing temperature for the hybrid material. In addition, EDS mapping for Al, Zn and Mn elements of the selected area in the AZ31 region annealed at 523 K (Figure 2b) shows the $Mg_{17}Al_{12}$, Mg_2Zn and Al_8Mn_5 phases and the STEM image in HAADF mode of the selected area in the Mg-0.6Gd region annealed at 623 K shows the $Mg_{12}Gd$ and Mg_5Gd phases (Figure 2c).

The microstructure of the hybrid material became more homogeneous after annealing at 723 K (Figure 2d) where the interface bonding is less visible and the precipitates dissolved in the Mg-0.6Gd region [20]. The average mean grain of the AZ31 and Mg-0.6Gd regions at 723 K reached values of 3.0 ± 0.3 and 5.3 ± 0.8 μm , respectively.

The mean grain size of the AZ31 and Mg-0.6Gd regions in the hybrid material can be used to examine the grain growth kinetics using the following equation [48]:

$$\frac{d^n - d_0^n}{t} = A \exp\left(\frac{-E_g}{RT}\right) \quad (2)$$

where d is the mean grain size at the annealing time of $t = 1$ h, d_0 is the initial mean grain size at $t = 0$ h corresponding to the deformation condition (taken as 0.30 ± 0.03 μm for the AZ31 region and 0.34 ± 0.02 μm for the Mg-0.6Gd region), n is the grain growth exponent which is related to the mobility and energy of the grain boundaries [49], A is the grain growth rate constant and E_g is the activation energy for grain growth that corresponds to the slope of a plot of $\ln(d^n - d_0^n)$ against $1000/RT_p$.

The grain growth exponent n is determined by analysing the slope of the curve of $\ln(dd/dt)$ as a function of $\ln(d)$ where, for the material without defects, n should be equal to 2. Unfortunately, an experimental determination of n was not possible for these results because isothermal annealing was not performed. Based on previous investigations, the grain growth exponent for various deformed Mg-based alloys is often in the range of 2–4 [40, 50–55] although some investigations reported much higher values such as $n = 8$ [42, 56]. The presence of microstructural heterogeneities including the presence of solute drag, dislocation substructure and the grain orientation is responsible for the deviation of n from the ideal value [42, 57].

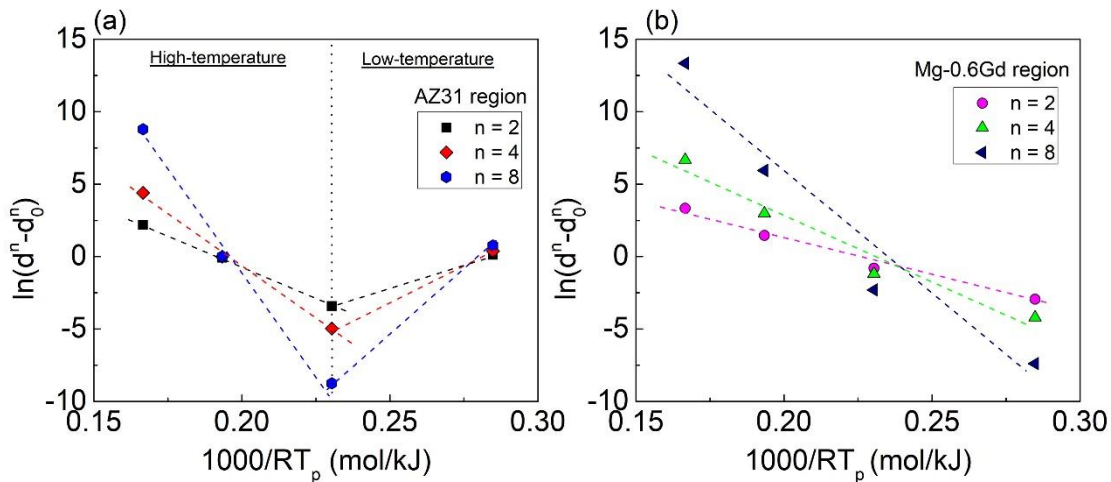


Figure 3: Evolution of $\ln(d^n - d_0^n)$ as a function of $1000/RT_p$ with different grain growth exponents ($n = 2, 4$ and 8) for (a) AZ31 and (b) Mg-0.6Gd regions of the hybrid material.

Hence, the activation energy for the present results was calculated by separately assuming $n = 2, 4$ and 8 . Figure 3 shows the evolution of $\ln (d^n - d_0^n)$ as a function of $1000/RT_p$ with these different grain growth exponents for the AZ31 and Mg-0.6Gd regions of the hybrid material, respectively. It is evident that the plot of the AZ31 region can be separated into two stages which may be identified as the low-temperature and high-temperature stages. The precipitation of the $Mg_{17}Al_{12}$ and Mg_2Zn phases hindered grain growth in the low-temperature stage and therefore the activation energy in this stage was not considered since it has no physical meaning. An AZ31 alloy processed by equal channel angular pressing [58] and HPT-processed Mg-1.4Nd (wt.%) alloy [59] were also shown to have two distinct ranges of grain growth activation energy. By contrast, the plot for the Mg-0.6Gd region (Figure 3b) can be well fitted by a single line and this confirms that the precipitation of the Mg_5Gd and $Mg_{12}Gd$ phases does not affect the grain growth process. This result demonstrates that the nature of both the second phase and the solute element play a key role in controlling the grain growth process in Mg composite materials.

Table 1 summarizes the values of the activation energy for grain growth with different n values for the AZ31 and Mg-0.6Gd regions of the hybrid material. Using $n = 2$ gives values for the activation energy for both the AZ31 (88.2 ± 1.3 kJ/mol) and Mg-0.6Gd (52.7 ± 5.1 kJ/mol) regions that are lower than the activation energy for grain boundary diffusion in pure Mg (~ 92 kJ/mol). It is reasonable to anticipate that the value of $n = 2$ underestimates the real activation energy since, as already noted, n is equal to 2 for materials with no defects. However, the evolution of the microstructures of both the AZ31 and the Mg-0.6Gd regions shown in Figure 2 and the former reports [19-21, 28] demonstrate that the alloys are far removed from a material without defects and microstructural heterogeneity.

Table 1. Activation energy for grain growth of hybrid AZ31/Mg-0.6Gd material using different grain growth exponents ($n = 2, 4$ and 8).

E_g (kJ/mol)	$n = 2$	$n = 4$	$n = 8$
AZ31 region	88.2 ± 1.3	146.2 ± 8.4	272.7 ± 25.6
Mg-0.6Gd region	52.7 ± 5.1	90.9 ± 13.5	173.1 ± 30.6

When $n = 4$, the activation energy in the AZ31 region of 146.2 ± 8.4 kJ/mol is close to the activation energy for lattice self-diffusion in pure Mg (~ 135 kJ/mol). For the Mg-0.6Gd region, the activation energy of 90.9 ± 13.5 kJ/mol corresponds to the activation energy for grain

boundary diffusion in pure Mg (~ 92 kJ/mol). The activation energies when $n = 8$ are equal to 272.7 ± 25.6 and 173.1 ± 30.6 kJ/mol in the AZ31 and Mg-0.6Gd regions, respectively, and these values are significantly higher than the activation energy for lattice self-diffusion in pure Mg which suggests that a value of $n = 8$ overestimates the real activation energy.

Usually, the activation energy for grain growth of the AZ31 alloy is in the range of 92–115 kJ/mol [42, 50, 55] and the high activation energy in the present analysis appears to be associated with the precipitates ($Mg_{17}Al_{12}$ and Mg_2Zn) and the segregation of the Zn element at the grain boundaries [20]. This precipitation was also the origin of the high grain growth activation energy of ~ 147 kJ/mol in the temperature range of 523–723 K for an HPT-processed Mg-1.4Nd (wt.%) alloy [59]. The lower activation energy for the Mg-0.6Gd region is reasonable because the grain growth process occurred in a microstructure which was already dynamically recrystallized and contained a low dislocation density [58].

The difference in the recrystallization and grain growth mechanisms found for the AZ31 and Mg-0.6Gd regions confirms the heterogeneous thermal stability of this hybrid AZ31/Mg-0.6Gd material. Thus, these results provide useful information for tailoring and appropriately adjusting the processing of new Mg-based composites.

4. Summary and conclusions

The activation energy for recrystallization of the hybrid AZ31/Mg-0.6Gd material fabricated by HPT processing through 20 turns was calculated using DSC analyses. In addition, the activation energies for grain growth were estimated using microstructural observations after isochronal annealing at 423, 523, 623 and 723 K for 1 h. The key conclusions are as follows:

- The exothermic peak in the hybrid material is attributed to the recrystallization of the AZ31 region. The activation energy of recrystallization was estimated as 112 ± 10 kJ/mol which falls between the activation energies for bulk and grain boundary diffusion.
- The precipitation of $Mg_{17}Al_{12}$ and Mg_2Zn phases in the AZ31 region significantly obstructs the grain growth process in the low-temperature range of 423–523 K. By contrast, the impact of precipitation of Mg_5Gd and $Mg_{12}Gd$ phases on grain growth of the Mg-0.6Gd region is less evident due to their development after complete recrystallization and grain growth.

- The activation energies for grain growth in the AZ31 and Mg-0.6Gd regions with grain growth exponent of $n = 4$ were found equal to 146.2 ± 8.4 and 90.9 ± 13.5 kJ/mol, respectively.

Acknowledgements

The authors sincerely thank Drs. N. Hort and D. Letzig (MagIC, Germany) and Dr. T. Al-Samman (RWTH-Aachen University, Germany) for supplying the AZ31 and Mg-0.6Gd alloys, respectively. The European Research Council provided funding for YH and TGL under Grant Agreement No. 267464-SPDMETALS. PB was supported by the National Science Centre Poland under Grant Agreement No. 2020/37/B/ST5/01837.

Conflict of Interest

The authors declare no conflict of interest.

Data Availability Statement

Data will be made available on request.

References

- [1] I.M. Alarifi, R. Asmatulu, 4 - Matrix hybrid composite materials, in: I.M. Alarifi, R. Asmatulu (Eds.) *Advanced Hybrid Composite Materials and their Applications*, Woodhead Publishing, Cambridge, U.K., 2023, pp. 67-88.
- [2] S.K. Khatkar, Hybrid magnesium matrix composites: A review of reinforcement philosophies, mechanical and tribological characteristics, *RAMS*, 62 (2023) 20220294.
- [3] Y. Chen, Z. Xu, C. Smith, J. Sankar, Recent advances on the development of magnesium alloys for biodegradable implants, *Acta Biomater.*, 10 (2014) 4561-4573.
- [4] M.M. Zerankeshi, R. Alizadeh, E. Gerashi, M. Asadollahi, T.G. Langdon, Effects of heat treatment on the corrosion behavior and mechanical properties of biodegradable Mg alloys, *J. Magnes. Alloy*, 10 (2022) 1737-1785.
- [5] R.Z. Valiev, Y. Zheng, K. Edalati, Review: nanoSPD-produced metallic materials for advanced medical devices, *J. Mater. Sci.*, 59 (2024) 5681-5697.
- [6] R.Z. Valiev, I.V. Alexandrov, M. Kawasaki, T.G. Langdon, *Ultrafine-Grained Materials*, Springer International Publishing, Cham, Switzerland, 2024.
- [7] M.M. Castro, P.H.R. Pereira, A. Isaac, R.B. Figueiredo, T.G. Langdon, Development of a magnesium-alumina composite through cold consolidation of machining chips by high-pressure torsion, *J. Alloys Compd.*, 780 (2019) 422-427.
- [8] M.M. Castro, D.R. Lopes, R.B. Soares, D.M.M. dos Santos, E.H.M. Nunes, V.F.C. Lins, P.H.R. Pereira, A. Isaac, T.G. Langdon, R.B. Figueiredo, Magnesium-Based Bioactive Composites Processed at Room Temperature, *Mater.*, 12 (2019) 2609.
- [9] D. Lopes, R.B. Soares, M.M. Castro, R.B. Figueiredo, T.G. Langdon, V.F.C. Lins, Corrosion Behavior in Hank's Solution of a Magnesium–Hydroxyapatite Composite Processed by High-Pressure Torsion, *Adv. Eng. Mater.*, 22 (2020) 2000765.

- [10] M.M. Castro, P.H.R. Pereira, A. Isaac, T.G. Langdon, R.B. Figueiredo, Inverse Hall–Petch Behaviour in an AZ91 Alloy and in an AZ91–Al₂O₃ Composite Consolidated by High-Pressure Torsion, *Adv. Eng. Mater.*, 22 (2020) 1900894.
- [11] B. Ahn, A.P. Zhilyaev, H.-J. Lee, M. Kawasaki, T.G. Langdon, Rapid synthesis of an extra hard metal matrix nanocomposite at ambient temperature, *Mater. Sci. Eng. A*, 635 (2015) 109-117.
- [12] M. Kawasaki, B. Ahn, H. Lee, A.P. Zhilyaev, T.G. Langdon, Using high-pressure torsion to process an aluminum–magnesium nanocomposite through diffusion bonding, *J. Mater. Res.*, 31 (2016) 88-99.
- [13] J.-K. Han, K.-D. Liss, T.G. Langdon, M. Kawasaki, Synthesis of a bulk nanostructured metastable Al alloy with extreme supersaturation of Mg, *Sci. Rep.*, 9 (2019) 17186.
- [14] J.-K. Han, K. Sugimoto, M. Kawasaki, K.-D. Liss, Strain-dependent phase transformation mapping of diffusion-bonded nanocrystalline aluminum-magnesium by high-energy synchrotron X-rays, *Mater. Lett.*, 321 (2022) 132414.
- [15] D. Hernández-Escobar, Z.U. Rahman, H. Yilmazer, M. Kawasaki, C.J. Boehlert, Microstructural evolution and intermetallic formation in Zn-Mg hybrids processed by High-Pressure Torsion, *Philos. Mag.*, 99 (2019) 557-584.
- [16] M.M. Castro, L.A. Montoro, A. Isaac, M. Kawasaki, R.B. Figueiredo, Mechanical mixing of Mg and Zn using high-pressure torsion, *J. Alloys Compd.*, 869 (2021) 159302.
- [17] D. Hernández-Escobar, J. Marcus, J.-K. Han, R.R. Unocic, M. Kawasaki, C.J. Boehlert, Effect of post-deformation annealing on the microstructure and micro-mechanical behavior of Zn–Mg hybrids processed by High-Pressure Torsion, *Mater. Sci. Eng. A*, 771 (2020) 138578.
- [18] D. Hernández-Escobar, R.R. Unocic, M. Kawasaki, C.J. Boehlert, High-pressure torsion processing of Zn–3Mg alloy and its hybrid counterpart: A comparative study, *J. Alloys Compd.*, 831 (2020) 154891.
- [19] O. Ould Mohamed, H. Azzeddine, Y. Huang, T. Baudin, P. Bazarnik, F. Brisset, M. Kawasaki, T.G. Langdon, Investigation of Microstructure and Texture Evolution in an AZ31/Mg–Gd Alloy Hybrid Metal Fabricated by High-Pressure Torsion, *Adv. Eng. Mater.*, 25 (2023) 2201794.
- [20] O. Ould Mohamed, P. Bazarnik, Y. Huang, H. Azzeddine, T. Baudin, F. Brisset, M. Kawasaki, T.G. Langdon, Primary recrystallization of a magnesium hybrid material fabricated by high-pressure torsion, *Mater. Today Commun.*, 38 (2024) 108305.
- [21] T. Baudin, H. Azzeddine, F. Brisset, Y. Huang, T.G. Langdon, Estimating dislocation density from electron backscatter diffraction data for an AZ31/Mg-0.6Gd hybrid alloy fabricated by high-pressure torsion, *Philos. Mag.*, 104 (2024) 389-405.
- [22] R.B. Figueiredo, P.R. Cetlin, T.G. Langdon, Using finite element modeling to examine the flow processes in quasi-constrained high-pressure torsion, *Mater. Sci. Eng. A*, 528 (2011) 8198-8204.
- [23] A. Sheikhan, R. Roumina, R. Mahmudi, Texture softening in a rare earth elements-containing AZ31 magnesium alloy during hot compression deformation, *J. Mater. Res. Technol.*, 18 (2022) 4089-4098.
- [24] Z. Horita, K. Ohashi, T. Fujita, K. Kaneko, T.G. Langdon, Achieving High Strength and High Ductility in Precipitation-Hardened Alloys, *Adv. Mater.*, 17 (2005) 1599-1602.
- [25] G. Sha, Y.B. Wang, X.Z. Liao, Z.C. Duan, S.P. Ringer, T.G. Langdon, Influence of equal-channel angular pressing on precipitation in an Al–Zn–Mg–Cu alloy, *Acta Mater.*, 57 (2009) 3123-3132.
- [26] H. Azzeddine, B. Mehdi, L. Hennem, D. Thiaudière, B. Alili, M. Kawasaki, D. Bradai, T.G. Langdon, An in situ synchrotron X-ray diffraction study of precipitation kinetics in a severely deformed Cu–Ni–Si alloy, *Mater. Sci. Eng. A*, 597 (2014) 288-294.

- [27] L.L. Rokhlin, Magnesium alloys containing rare earth metals: structure and properties, First ed., Crc Press, London, 2003.
- [28] O. Ould Mohamed, P. Bazarnik, Y. Huang, H. Azzeddine, T. Baudin, F. Brisset, T.G. Langdon, A comparative study between AZ31 and Mg-Gd alloys after high-pressure torsion, *J. Mater. Eng. Perform.*, 33 (2024) 2860-2874.
- [29] J. Zhang, W. Li, Z. Guo, Static recrystallization and grain growth during annealing of an extruded Mg–Zn–Zr–Er magnesium alloy, *J. Magnes. Alloy*, 1 (2013) 31-38.
- [30] I. Basu, K.G. Pradeep, C. Mießen, L.A. Barrales-Mora, T. Al-Samman, The role of atomic scale segregation in designing highly ductile magnesium alloys, *Acta Mater.*, 116 (2016) 77-94.
- [31] Y.I. Bourezg, D. Elfiad, H. Azzeddine, D. Bradai, Investigation of recrystallization kinetics in hot-rolled Mg-La alloy using differential scanning calorimetry technique, *Thermochim. Acta*, 690 (2020) 178688.
- [32] F. Guerza-Soualah, A. Hanna, H. Azzeddine, A.-L. Helbert, F. Brisset, T. Baudin, D. Bradai, The deformation and recrystallization behaviour of an Mg-Dy alloy processed by plane strain compression, *Mater. Today Commun.*, 24 (2020) 101239.
- [33] F. Guerza-Soualah, H. Azzeddine, T. Baudin, A.-L. Helbert, F. Brisset, D. Bradai, Microstructural and textural investigation of an Mg–Dy alloy after hot plane strain compression, *J. Magnes. Alloy*, 8 (2020) 1198-1207.
- [34] N. Stanford, M.D. Callaghan, B. de Jong, The effect of rare earth elements on the behaviour of magnesium-based alloys: Part 1—Hot deformation behaviour, *Mater. Sci. Eng. A*, 565 (2013) 459-468.
- [35] S. Sandlöbes, M. Friák, S. Zaeferrer, A. Dick, S. Yi, D. Letzig, Z. Pei, L.F. Zhu, J. Neugebauer, D. Raabe, The relation between ductility and stacking fault energies in Mg and Mg–Y alloys, *Acta Mater.*, 60 (2012) 3011-3021.
- [36] Y.I. Bourezg, H. Azzeddine, K. Abib, Y. Huang, D. Bradai, T.G. Langdon, Recrystallization in an Mg-Nd alloy processed by high-pressure torsion: a calorimetric analysis, *J. Mater. Res. Technol.*, 9 (2020) 3047-3054.
- [37] A. Hanna, H. Azzeddine, Y. Huang, D. Bradai, J.M. Cabrera, T.G. Langdon, An investigation of the thermal stability of an MgDy alloy after processing by high-pressure torsion, *Mater. Charact.*, 151 (2019) 519-529.
- [38] P.G. Boswell, On the calculation of activation energies using a modified Kissinger method, *J. Therm. Anal.*, 18 (1980) 353-358.
- [39] H.J. Frost, M.F. Ashby, Deformation-mechanism Maps: The Plasticity and Creep of Metals and Ceramics, First Edition ed., Oxford, New York : Pergamon Press, 1982.
- [40] H.Y. Chao, H.F. Sun, W.Z. Chen, E.D. Wang, Static recrystallization kinetics of a heavily cold drawn AZ31 magnesium alloy under annealing treatment, *Mater. Charact.*, 62 (2011) 312-320.
- [41] H. Zhao, P.-j. Li, L.-j. He, Kinetics of recrystallization for twin-roll casting AZ31 magnesium alloy during homogenization, *Int. J. Min. Met. Mater.*, 18 (2011) 570-575.
- [42] S. Sadi, A. Hanna, T. Baudin, A.-L. Helbert, F. Brisset, D. Bradai, H. Azzeddine, Evaluation of static recrystallization and grain growth kinetics of hot-rolled AZ31 alloy, *Journal of Metals, Materials and Minerals*, 32 (2022) 12-26.
- [43] Y.I. Bourezg, H. Azzeddine, Y. Huang, D. Bradai, T. Langdon, Investigation of recrystallization kinetics by DSC analysis of Mg-Ce alloy after severe plastic deformation, in: 26th International Conference on Metallurgy and Materials (Metal 2017), Tanager Ltd, Brno, Czech Republic, EU, 2017, pp. 1524-1530.
- [44] J. Čížek, I. Procházka, B. Smola, I. Stulíková, V. Očenášek, R.K. Islamgaliev, O.B. Kulyasova, The Enhanced Kinetics of Precipitation Effects in Ultra Fine Grained Mg Alloys Prepared by High Pressure Torsion, *Defect and Diffusion Forum*, 273-276 (2008) 75-80.

- [45] O. Melikhova, J. Čížek, P. Hruška, M. Vlček, I. Procházka, M. Vlach, I. Stulíková, B. Smola, N. Žaludová, R.K. Islamgaliev, Influence of Deformation on Precipitation Kinetics in Mg-Tb Alloy, *Defect and Diffusion Forum*, 322 (2012) 151-162.
- [46] Y.I. Bourezg, H. Azzeddine, L. Hennet, D. Thiaudière, Y. Huang, D. Bradai, T.G. Langdon, The sequence and kinetics of pre-precipitation in Mg-Nd alloys after HPT processing: A synchrotron and DSC study, *J. Alloys Compd.*, 719 (2017) 236-241.
- [47] X. Liu, Y. Li, Y. Man, J. Wang, R. Xu, Precipitation and recrystallization of HPT-processed Mg-Sm-Ca alloy at low temperatures, *Mater. Lett.*, 277 (2020) 128252.
- [48] J.E. Burke, D. Turnbull, Recrystallization and grain growth, *Prog. Phys. Met.*, 3 (1952) 220-292.
- [49] A. Kazaryan, Y. Wang, S.A. Dregia, B.R. Patton, Grain growth in anisotropic systems: comparison of effects of energy and mobility, *Acta Mater.*, 50 (2002) 2491-2502.
- [50] C.W. Su, L. Lu, M.O. Lai, Mechanical behaviour and texture of annealed AZ31 Mg alloy deformed by ECAP, *Mater. Sci. Technol.*, 23 (2007) 290-296.
- [51] C.W. Su, L. Lu, M.O. Lai, Recrystallization and grain growth of deformed magnesium alloy, *Philos. Mag.*, 88 (2008) 181-200.
- [52] M. Roostaei, M. Shirdel, M.H. Parsa, R. Mahmudi, H. Mirzadeh, Microstructural evolution and grain growth kinetics of GZ31 magnesium alloy, *Mater. Charact.*, 118 (2016) 584-592.
- [53] Z. Jin, D. Yu, X. Wu, K. Yin, K. Yan, Drag Effects of Solute and Second Phase Distributions on the Grain Growth Kinetics of Pre-Extruded Mg-6Zn Alloy, *J. Mater. Sci Technol.*, 32 (2016) 1260-1266.
- [54] C.J. Silva, A. Kula, R.K. Mishra, M. Niewczas, Grain growth kinetics and annealed texture characteristics of Mg-Sc binary alloys, *J. Alloys Compd.*, 687 (2016) 548-561.
- [55] Q. Wang, B. Jiang, A. Tang, J. Fu, Z. Jiang, H. Sheng, D. Zhang, G. Huang, F. Pan, Unveiling annealing texture formation and static recrystallization kinetics of hot-rolled Mg-Al-Zn-Mn-Ca alloy, *J. Mater. Sci Technol.*, 43 (2020) 104-118.
- [56] M.A. Thein, L. Lu, M.O. Lai, Kinetics of grain growth in nanocrystalline magnesium-based metal-metal composite synthesized by mechanical alloying, *Compos. Sci. Technol.*, 66 (2006) 531-537.
- [57] G.T. Higgins, Grain-Boundary Migration and Grain Growth, *Met. Sci.*, 8 (1974) 143-150.
- [58] H.-K. Kim, Activation energies for the grain growth of an AZ31 Mg alloy after equal channel angular pressing, *J. Mater. Sci.*, 39 (2004) 7107-7109.
- [59] S. Tighiouaret, R. Lachhab, A. Hanna, H. Azzeddine, Y. Huang, T. Baudin, A.-L. Helbert, F. Brisset, D. Bradai, T.G. Langdon, Thermal Stability of an Mg-Nd Alloy Processed by High-Pressure Torsion, *Adv. Eng. Mater.*, 21 (2019) 1900801.